Effects of phosphorylation on Drp1 activation by its receptors, actin, and cardiolipin

Ao Liu[†], Anna L. Hatch[†,‡], and Henry N. Higgs[*]
Department of Biochemistry and Cell Biology, Geisel School of Medicine at Dartmouth, Hanover NH 03755

ABSTRACT **Drp1 is a dynamin family GTPase required for mitochondrial and peroxisomal division. Oligomerization increases Drp1 GTPase activity through interactions between neighboring GTPase domains. In cells, Drp1 is regulated by several factors including Drp1 receptors, actin filaments, cardiolipin, and phosphorylation at two sites: S579 and S600. Commonly, phosphorylation of S579 is considered activating, while S600 phosphorylation is considered inhibiting. However, direct effects of phosphorylation on Drp1 GTPase activity have not been investigated in detail. Here, we compare effects of S579 and S600 phosphorylation on purified Drp1, using phosphomimetic mutants and in vitro phosphorylation. Both phosphomimetic mutants are shifted toward smaller oligomers. Both phosphomimetic mutations maintain basal GTPase activity, but eliminate GTPase stimulation by actin and decrease GTPase stimulation by cardiolipin, Mff, and MiD49. Phosphorylation of S579 by Erk2 produces similar effects. When mixed with wildtype Drp1, both S579D and S600D phosphomimetic mutants reduce the actin-stimulated GTPase activity of Drp1-WT. Conversely, a Drp1 mutant (K38A) lacking GTPase activity stimulates Drp1-WT GTPase activity under both basal and actin-stimulated conditions. These results suggest that the effect of S579 phosphorylation is not to activate Drp1 directly. In addition, our results suggest that nearest neighbor interactions within the Drp1 oligomer affect catalytic activity.**

Monitoring Editor
Laurent Blanchoin
CEA Grenoble

Received: Nov 13, 2023
Accepted: Nov 20, 2023

SIGNIFICANCE STATEMENT

- Mammalian Drp1 is commonly known to be phosphorylated in two positions, S579 and S600, with S579 considered to be activating and S600 considered to be inhibitory to Drp1 function in mitochondrial fission. The direct effects of these phosphorylations on Drp1 biochemically, however, have not been examined in detail.
- We show that both S579 and S600 phosphorylation and/or phosphomimetics decrease the GTPase activity of purified Drp1 in several contexts.
- These results suggest that other factors must contribute to phosphorylation-based Drp1 regulation in cells, especially for S579.

This article was published online ahead of print in MBoC in Press (http://www.molbiolcell.org/cgi/doi/10.1091/mbc.E23-11-0427) on November 29, 2023.

[†]These authors contributed equally to this publication.

[‡]Present address: 4000 Jones Bridge Road, Chevy Chase MD 20815-6789

*Address correspondence to: Henry N. Higgs (henry.higgs@dartmouth.edu).

Abbreviations used: ATP, adenosine triphosphate; BSE, bundle signaling element; CL, cardiolipin; GDP, guanosine diphosphate; GTP, guanosine triphosphate; NDPK, nucleotide diphosphate kinase; PKA, protein kinase A; VD, variable domain; WT, wild-type.

INTRODUCTION

The dynamin family GTPase Drp1 is an important mediator of membrane fission for at least two organelles, mitochondria and peroxisomes (Kraus *et al.*, 2021). When not mediating membrane fission, Drp1 is a cytoplasmic protein. To induce membrane fission, Drp1 is recruited to the target membrane by receptor proteins, where it oligomerizes into a ring structure around the membrane. Oligomerization increases Drp1 GTPase activity by bringing the N-terminal GTPase domains into close proximity (Bui and Shaw, 2013; Fröhlich *et al.*, 2013; Koirala *et al.*, 2013). Guanosine triphosphate (GTP) hydrolysis results in constriction of the Drp1 ring and membrane constriction.

Drp1 receptors can directly activate Drp1. One Drp1 receptor, Mff, is on both mitochondrial and peroxisomal membranes. Mff itself is a trimer, and its binding causes increased Drp1 GTPase activity in vitro (Clinton *et al.*, 2016; Liu *et al.*, 2021). A second set of Drp1 receptors, MiD49 and MiD51, are only found on mitochondria. In their inactive state, MiD proteins are monomeric and do not activate Drp1. Binding to fatty acyl-coenzyme A stimulates MiD oligomerization, which in turn stimulates Drp1 GTPase activity (Liu *et al.*, 2023).

Other regulatory molecules for Drp1 include actin filaments and phospholipids. Biochemically, actin filaments stimulate Drp1 GTPase activity approximately four-fold through direct binding (Ji *et al.*, 2015; Hatch *et al.*, 2016). In cells, actin polymerization through an endoplasmic reticulum-bound formin protein, INF2, increases Drp1 oligomerization and mitochondrial recruitment (Korobova *et al.*, 2013; Ji *et al.*, 2015, 2017). The mitochondrial lipid cardiolipin (CL) can affect a >20-fold stimulation of GTPase activity biochemically (Macdonald *et al.*, 2014), while CL-derived phosphatidic acid suppresses Drp1 activation (Adachi *et al.*, 2016).

Drp1 is also subject to a number of posttranslational modifications (Chang and Blackstone, 2010; Wilson *et al.*, 2013), with phosphorylation in particular being correlated with changes in Drp1-mediated mitochondrial fission. Two well-studied phosphorylation sites occur within a 21 amino acid segment of the Variable Domain (VD) of Drp1 (Wilson *et al.*, 2013; Figure 1A), which forms an unstructured loop at one end of the elongated Drp1 structure (Fröhlich *et al.*, 2013; Figure 1B). Depending on the splice variant and species studied (Strack *et al.*, 2013; Itoh *et al.*, 2018; Rosdah *et al.*, 2020), the positions of these sites differ (Figure 1C), with the most common names in the literature being S616 and S637, but which will be referred to here mostly as S579 and S600, as explained in the *Results* section.

Phosphorylation of S579 has been observed for multiple kinases, including CDK1, CDK5, ERK2, CaMKII, ROCK, PKCδ, and PINK (Taguchi *et al.*, 2007; Qi *et al.*, 2011; Yu *et al.*, 2011; Strack *et al.*, 2013; Kashatus *et al.*, 2015; Serasinghe *et al.*, 2015; Xu *et al.*, 2016; Brand *et al.*, 2018; Han *et al.*, 2020), with phosphorylation being correlated with increased mitochondrial fission. Phosphorylation of S600 by protein kinase A (PKA), CaMK1a, ROCK1, AMPK, and protein kinase D has been reported (Chang and Blackstone, 2007; Cribbs and Strack, 2007; Han *et al.*, 2008; Wang *et al.*, 2012; Wikstrom *et al.*, 2013; Jhun *et al.*, 2018). In most cases, S600 phosphorylation has been correlated with decreased mitochondrial fission (Chang and Blackstone, 2007; Cribbs and Strack, 2007; Cereghetti *et al.*, 2008; Wikstrom *et al.*, 2013). However, some studies show evidence for a positive effect of S600 phosphorylation on cellular Drp1 activity (Han *et al.*, 2008; Wang *et al.*, 2012; Jhun *et al.*, 2018; Galvan *et al.*, 2019), while another study reports no effect (Yu *et al.*, 2019). Finally, one report suggests that S600 phosphorylation promotes S579 phosphorylation, and that the doubly phosphorylated S579/S600 protein correlates with increased mitochondrial fission (Valera-Alberni *et al.*, 2021). Many of the above-cited publications utilize phosphomimetic mutants to induce similar mitochondrial changes to those induced by phosphorylation, suggesting that phosphomimetics can elicit similar effects.

It is unclear whether phosphorylation at either site directly alters Drp1 activity. For S579 phosphorylation, no biochemical data addressing Drp1 activity are available. For S600 phosphorylation, the biochemical data are conflicting. In one study, a phosphomimetic mutant of Drp1 maintains oligomerization and GTP hydrolysis activity (Cribbs and Strack, 2007). In another study, in vitro phosphorylation of GST-Drp1 by PKA inhibits GTPase activity (Chang and Blackstone, 2007). Recent structural work suggests that S600 phosphorylation inhibits MiD49 binding (Kalia *et al.*, 2018), although cellular co-IP experiments suggest that the S600D phosphomimetic binds better to MiD49 and MiD51 than does the nonphosphorylatable S600A mutant (Losón *et al.*, 2013). Other studies show that the region of Drp1 containing both phosphorylation sites (the VD) inhibits binding to Mff (Liu and Chan, 2015; Clinton *et al.*, 2016), although neither S579D nor S600D phosphomimetics alter this effect (Liu and Chan, 2015).

In this study, we assess the biochemical effects of Drp1 phosphorylation on oligomerization and GTPase activity of Drp1 alone, and in the presence of several activators (actin, CL, Mff, MiD49). For these studies, we use both phosphomimetic S-to-D mutations and in vitro phosphorylation on the S579 site. Surprisingly, we find that both types of phosphorylation inhibit the abilities of these activators to stimulate Drp1 activity.

RESULTS

Phosphomimetic mutants are less oligomerized in the nucleotide-free state

We constructed two phosphomimetic Drp1 mutants corresponding to S616D and S637D in isoform 1. We refer to these mutants, however, as S579D and S600D, respectively, because we use isoform 3 of Drp1 (Figure 1C). In HeLa, HL60 and PC12 cells, isoform 3 is the most abundant isoform present, making up over 40% of total Drp1 protein (Strack *et al.*, 2013). In another study, isoform 3 represents the majority of the mRNA in mouse heart, muscle, liver, and embryonic fibroblasts, and is the most ubiquitously expressed isoform throughout tissues (Itoh *et al.*, 2018).

The S579 site, generally thought to activate Drp1, is located within the VD; while the S600 site, generally thought to inhibit Drp1, marks the boundary between the VD and the stalk (Figure 1A). The region encompassing both sites is poorly resolved in the existing structural models of nucleotide-free Drp1(Fröhlich *et al.*, 2013; Figure 1B) or other models (Kalia *et al.*, 2018).

By size exclusion chromatography at high Drp1 concentration (30 μM), both phosphomutants are slightly shifted to smaller sizes compared with Drp1-WT (Figure 2A). For more detailed analysis of Drp1 hydrodynamic properties, we used velocity analytical ultracentrifugation (vAUC). Previously, we reported that purified Drp1-WT exists in several oligomeric states (Hatch *et al.*, 2016), similar to the results of other studies (Fröhlich *et al.*, 2013; Macdonald *et al.*, 2014). We compared the Drp1-S579D and Drp1-S600D to Drp1-WT by vAUC at three concentrations: 8, 4, and 1.5 μM (Figure 2B). As with Drp1-WT, both mutants display a 7 S species that is similar to the sedimentation pattern of an oligomerization-deficient mutant (Fröhlich *et al.*, 2013; Hatch *et al.*, 2016), suggesting that this is the dimeric species. In addition, several species of higher S values, corresponding to larger oligomers, are present for Drp1-WT. At all concentrations tested, both Drp1 S579D and S600D shift towards smaller oligomers when compared with WT, with the S600D mutant displaying a greater shift.

We also tested the ability of Drp1 to form larger oligomers in the presence of the nonhydrolysable GTP analogue GMP-PCP using a high-speed sedimentation assay (Hatch *et al.*, 2016). At three Drp1 concentrations (0.5, 1.0, and 2.0 μM), GMP-PCP causes similar degrees of Drp1 sedimentation for all constructs, suggesting that GTP-mediated oligomerization is not affected by these mutations (Figure 2, C and D).

These data suggest that both the S579D and S600D mutants display less ability to oligomerize in the nucleotide-free state than WT Drp1, but that nonhydrolyzable GTP induces all three proteins to oligomerize.

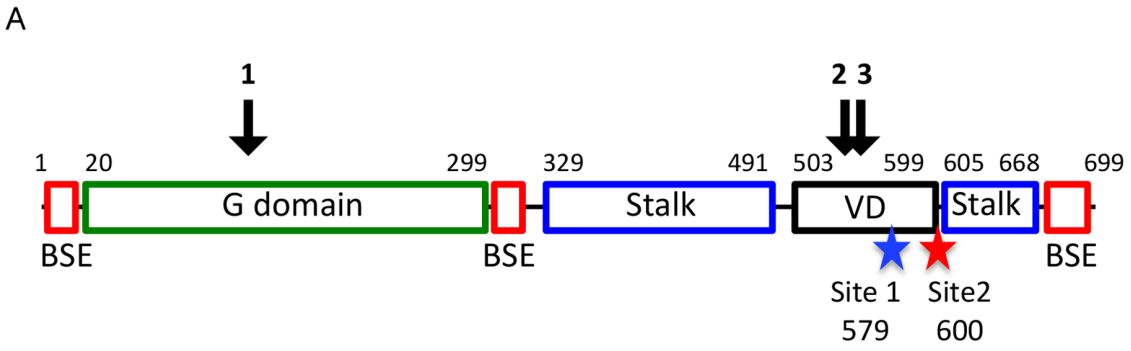

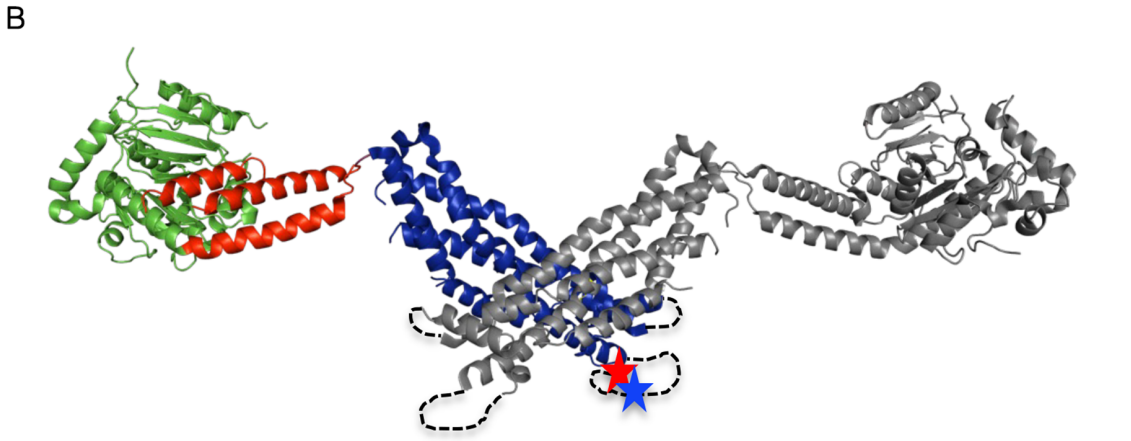

C

Isoform name*	Binary nomenclature**	UniProtKB	Protein length (amino acids)	Phosphorylation site 1	Phosphorylation site 2
isoform 1	0 1 1	o00042-1	736	616	637
isoform 2	0 0 1	o00429-3	710	590	611
isoform 3	0 0 0	o00429-4	699	579	600
isoform 4	0 1 0	o00429-2	725	605	626
isoform 5	0 x 0	o00429-5	710	590	611
isoform 6	1 1 1	o00429-6	749	629	650
isoform 7	x 1 1	o00429-7	533	413	434
isoform 8	1 1 0	o00429-8	738	618	639
isoform 9	1 0 0	o00429-9	712	592	613

FIGURE 1: Drp1 phosphorylation sites. (A) Domain organization of Drp1 isoform 3 (also called Drp1-000): GTPase domain (green), Bundle Signaling Element (BSE, red), stalk (blue), VD, black, also called the B-insert in some publications. Blue and red stars indicate phosphorylation sites S579 (site 1) and S600 (site 2), respectively. Black arrows indicate locations of the three alternatively spliced inserts. (B) Structural model of Drp1 dimer (PDB 4BEJ) showing positions of phosphorylation sites S579 (blue star) and S600 (red star) on one subunit (color coded similar to panel A). Dashed loops for VD denote that this was not resolved in PDB 4BEJ. (C) Table listing positions of the phosphorylation sites corresponding to S579 (Site 1) and S600 (Site 2) in this paper for the nine human Drp1 isoforms listed in UniProt, following: *isoform designation given by (Rosdah *et al.*, 2020) and, ** binary nomenclature used by (Strack *et al.*, 2013). Binary nomenclature based on presence (1) or absence (0) of the three alternatively spliced inserts, with "x" denoting a variation of the indicated site (described in [Rosdah *et al.*, 2020]). Of note, additional splice variants have been identified in murine Drp1 (Itoh *et al.*, 2018).

Phosphomimetic mutants for both S579 and S600 reduce Drp1 responses to activators

We next examined the GTPase activities of the two phosphomimetic mutants. Both mutants display similar GTPase activity to Drp1-WT (1.57 ± 0.09, 1.51 ± 0.02, and 1.33 ± 0.14 μM/min/μM for WT, S579D, and S600D, respectively). Previously, we reported that actin filaments have a biphasic effect on Drp1 GTPase activity, where low actin filament concentrations are stimulatory but higher concentrations bring the activity back to the Drp1-alone values (Hatch *et al.*, 2016), likely due to the fact that sparser Drp1 binding along the actin filament at high actin:Drp1 ratio reduces interaction between Drp1 GTPase domains (Liu *et al.*, 2023). We tested whether the phosphomimetic mutants responded to actin in a similar manner. Surprisingly, actin does not activate Drp1 S579D or Drp1 S600D at any concentration tested (Figure 3A).

Previously, we reported that Drp1 binds actin filaments with a K_d^{app} in the range of 1–2 μM (Ji *et al.*, 2015; Hatch *et al.*, 2016). We compared actin binding for Drp1-WT, Drp1-S579D, and Drp1-S600D by cosedimentation assay at two ionic strengths: 65 mM and 140 mM NaCl. Drp1-WT and Drp1-S579D display similar K_d for actin at 65 mM NaCl (K_d^{app} 1.7 and 2.5 μM for WT and S579D, respectively), while Drp1-S600D displays significantly lower actin affinity

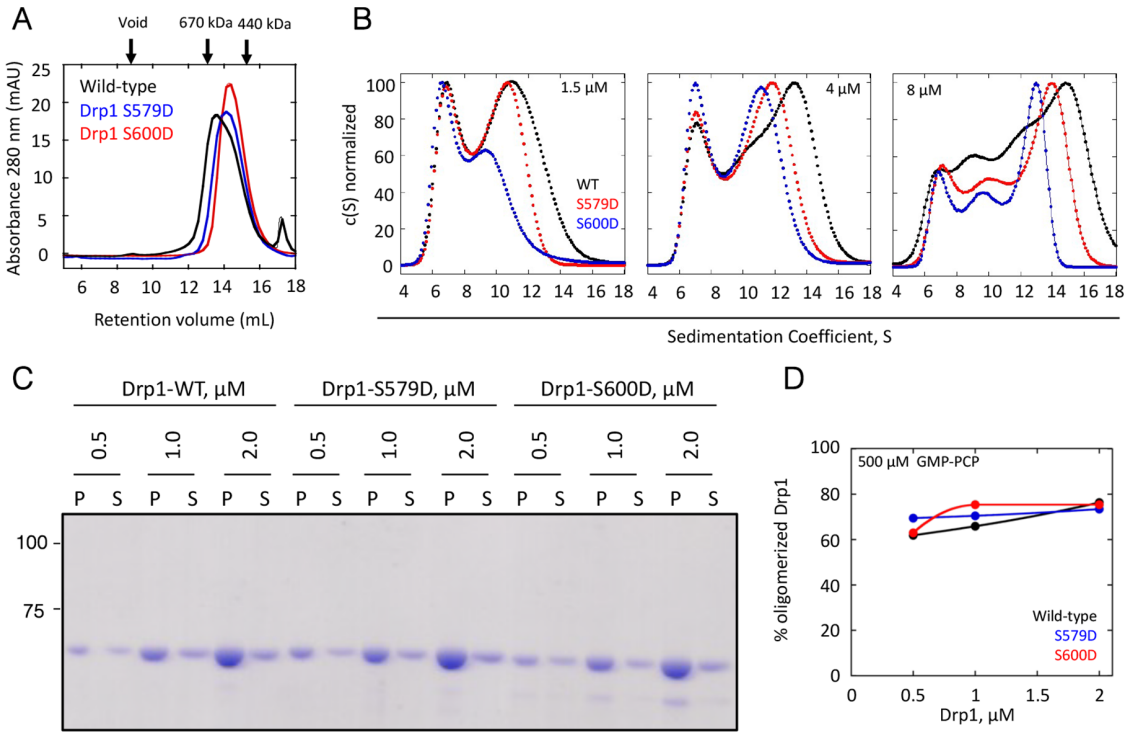

FIGURE 2: Oligomeric properties of Drp1 phosphomimetic mutants. (A) Superose 6 gel filtration profiles of 30 µM of Drp1-WT, Drp1-S579D, and Drp1-S600D. At top are peak elution positions for two standards (thyroglobulin [670 kDa] and ferritin [440 kDa]) as well as the void volume position. (B) vAUC of Drp1-WT, Drp1-S579D, and Drp1-S600D (black, red, and blue, respectively) at three concentrations: 8, 4, and 1.5 µM. (C) Coomassie-stained gel showing sedimentation assays graphed in panel C. Mass markers (in kDa) shown at left. P = pellet, S = supernatant. (D) Quantification of percent oligomerized Drp1 from sedimentation assays of Drp1-WT, Drp1-S579D, and Drp1-S600D in the presence of the nonhydrolysable GTP analogue GMP-PCP (500 µM) at 0.5, 1.0, and 2.0 µM Drp1.

(K_d^{app} 7.1 µM). We previously reported that Drp1-WT binding to actin filaments saturates at approximately 50% Drp1 bound (Hatch *et al.*, 2016). Both mutants display lower percent bound at saturating actin (48, 27, and 18% bound for WT, S579D, and S600D, respectively; Figure 3B; Supplemental Figure S1, A and B). At 140 mM NaCl, Drp1 S579D has a similar affinity for actin filaments as WT (1.1 and 1.2 µM for S579D and wild-type, respectively) and a comparable percent bound (10.9 and 8.3% for S579D and WT, respectively), while Drp1 S600 has lower affinity and percent bound than the other constructs (4.3 µM and 6.1% bound; Figure 3C; Supplemental Figure S1, C–E). These results suggest that the phosphosite mutants have altered actin-binding properties, with Drp1 S600D displaying less actin interaction under all conditions.

We also asked whether GTPase stimulation by another Drp1 activator, CL (Macdonald *et al.*, 2014), was affected by the S579D or S600D mutations. Interestingly, unilamellar vesicles containing 25 mol% CL are less stimulatory to Drp1-S579D and Drp1-S600D than they are for Drp1-WT (Figure 3D).

We have previously shown that the cytoplasmic region of the Drp1 receptor Mff activates Drp1, and that actin filaments synergize with Mff by reducing the Mff concentration needed for maximal Drp1 activation (Liu *et al.*, 2021). Both phosphomimetic mutants display slightly decreased activation by Mff alone (Figure 3E). Interestingly, actin filaments still synergize with Mff for Drp1-S579D stimulation, albeit with a lower maximal activation (Figure 3F). In contrast, the Drp1-S600D mutant displays greatly reduced synergy between actin and Mff (Figure 3F).

Two other Drp1 receptors, MiD49 and MiD51, do not activate Drp1 GTPase activity when they themselves are not activated. Upon binding their activating ligand, acyl-CoA, MiD proteins oligomerize, resulting in Drp1 GTPase activation in a biphasic manner, similar to actin (Liu *et al.*, 2023). Here, we find that both Drp1 phosphomimetic mutants are also activated by acyl-CoA-bound MiD49 in a biphasic manner. However, the degree of activation is lower, with Drp1-S600D being most affected (Figure 3G). Similar to Drp1-WT, neither phosphomimetic mutant is stimulated by MiD49 monomer (Figure 3G).

As with actin filaments, oligomerized MiD49 synergizes with Mff by reducing the Mff concentration required for maximal Drp1 activation. Drp1-S579D displays maximal activity in the presence of low concentrations of Mff and oligomerized MiD49, albeit at a lower maximum than Drp1-WT (Figure 3H). Similarly, despite its decreased ability to stimulate Drp1-S600D, oligomerized MiD49 is able to reduce the concentration of Mff required for Drp1-S600D stimulation.

One question is whether the phosphomimetic mutants bind Drp1 receptors with lower affinity, as opposed to binding similar affinity but being activated to a lower level. As a test of these possibilities, we used cosedimentation assays with Drp1 (WT, S579D, or S600D) and Mff in the presence of GMP-PCP. We use a concentration of Mff (50 µM) that causes a significant increase in Drp1 GTPase activity (Figure 3E). As observed earlier (Figure 1, C and D), GMP-PCP causes efficient sedimentation of all three Drp1 constructs (Supplemental Figure S2). When Mff is also present, GMP-PCP results in Mff sedimentation at approximately stoichiometric amounts to Drp1 (Supplemental Figure S2). These effects occur with all Drp1 constructs (WT, S579D, S600D), suggesting that Drp1 binding to Mff is not significantly compromised in the phosphomimetic mutants.

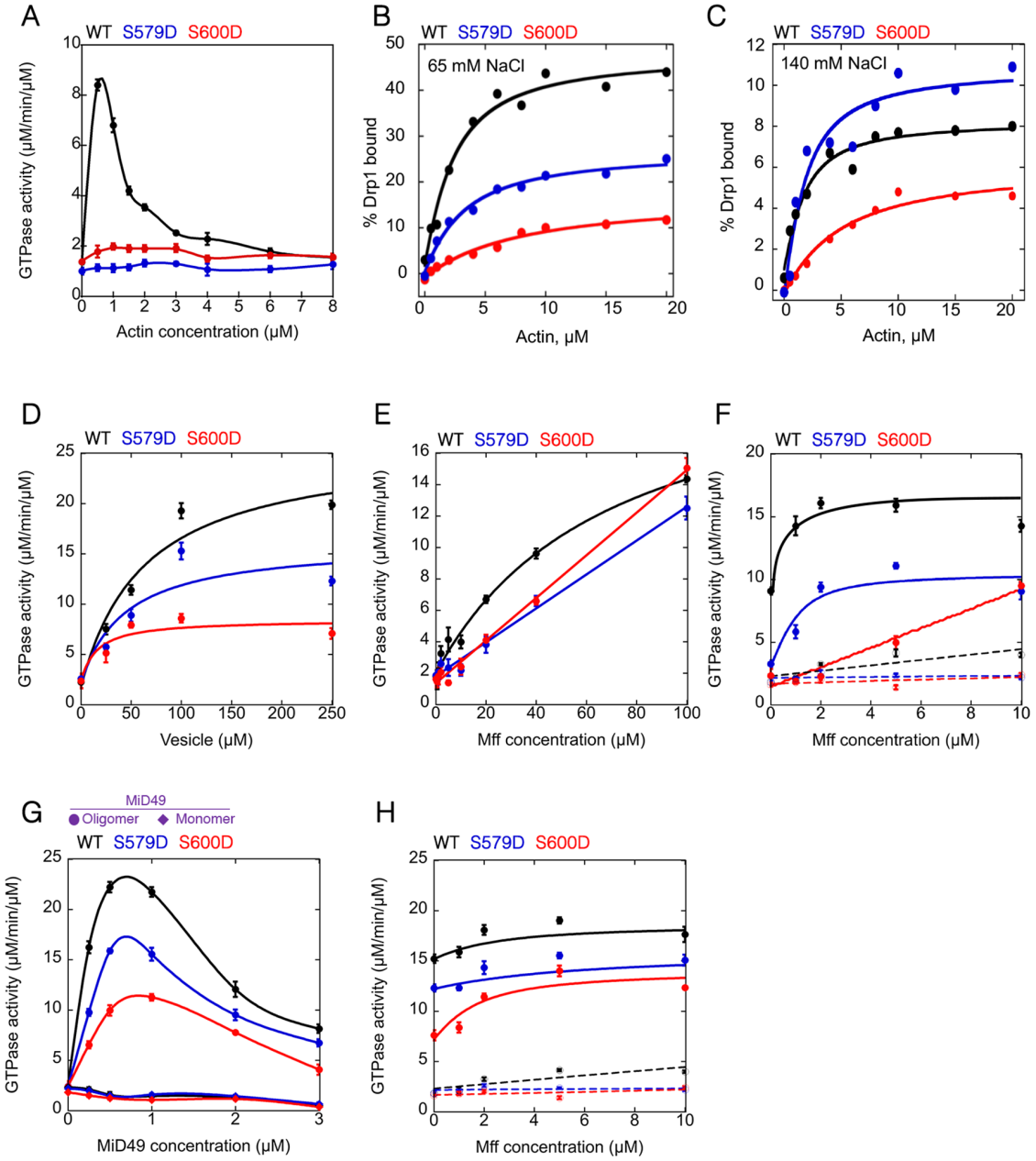

FIGURE 3: Effects of Drp1 phosphomimetic mutants on actin binding and GTPase stimulation by actin, Mff, and MiD49. Wild-type, Drp1 S579D, Drp1 S600D shown in black, blue, and red, respectively, for all panels. All GTPase assays contain 0.75 μM Drp1. (A) GTPase assays containing 0.75 μM Drp1 that was preincubated with the indicated concentration of actin filaments for 5 min before GTP addition. Activity expressed as μM phosphate released per minute per μM Drp1. (B) and (C) Graphs of percent Drp1 bound versus actin concentration, from cosedimentation assays at 65 mM (B) and 140 mM NaCl (C), respectively (1.3 μM Drp1 in all cases). Raw data in Supplemental Figure S1. (D) GTPase assays containing Drp1 that was preincubated with the indicated concentration of CL-containing vesicles (40% DOPC, 35% DOPE, 25% CL) for 5 min before GTP addition. (E) Comparison of Drp1-WT with Drp1-S579D and Drp1-S600D GTPase activities in the presence of the indicated concentration of Mff for 5 min before GTP addition. (F) Comparison of Drp1-WT with Drp1-S579D and Drp1-S600D GTPase activities in the presence of 0.5 μM actin filaments and the indicated concentration of Mff for 5 min before GTP addition. Values for Mff alone are indicated by open circles and dashed lines, while values for Mff/actin are indicated by closed circles and solid lines. (G) Comparison of Drp1-WT with Drp1-S579D and Drp1-S600D GTPase activities in the presence of the indicated concentration of MiD49 monomer (diamonds) or MiD49 oligomer (circles) for 5 min before GTP addition. (H) Comparison of Drp1-WT with Drp1-S579D and Drp1-S600D GTPase activities in the presence of 0.25 μM MiD49 oligomer and the indicated concentration of Mff for 5 min before GTP addition. Values for Mff alone are indicated by open circles and dashed lines, while values for Mff/MiD49 are indicated by closed circles and solid lines. Error bars represent mean ± S.D. ($n = 3$).

We conducted similar sedimentation experiments in the absence of nucleotide, or in the presence of GTP. In the absence of nucleotide, Mff does not result in significant sedimentation of any Drp1 construct (Supplemental Figure S2). In the presence of GTP, a low amount of Drp1 sediments in the absence of Mff, but this amount significantly increases in the presence of Mff (Supplemental Figure S2). Both mutants (S579D and S600D) display ~ 50% less Drp1 and Mff in these pellets than for Drp1-WT (Supplemental Figure S2), suggesting a decreased ability to oligomerize in the presence of GTP and Mff.

These results show that phosphomimetics of both the "activating" (S579D) and "inhibitory" (S600D) sites on Drp1 result in a reduction of Drp1 activation by a variety of activators. This reduction is most pronounced for actin filaments.

Drp1 phosphorylated on S579 displays similar properties to the S579D phosphomimetic

The results for Drp1-S579D were surprising, considering that this site has been found to be associated with increased mitochondrial fission in cells. We sought to test these results further by directly phosphorylating Drp1 on S579 using recombinant ERK2, one of the kinases shown to mediate this phosphorylation (Kashatus *et al.*, 2015; Serasinghe *et al.*, 2015) Incubation with ERK2 for 4-h results in a slight decrease in mobility on SDS–PAGE, suggestive of phosphorylation (Figure 4A). Western blotting using an antibody against phospho-S579 shows saturation of this signal on a similar time scale (Figure 4B). Size exclusion chromatography of 4-h phosphorylated Drp1 results in a similar elution profile to mock-phosphorylated sample (Figure 4C, 30 μM Drp1 loaded). Analysis by tryptic digest and mass spectrometry reveals that 81% of the detected phosphorylation events are on S579, with other phosphorylated residues detected being: S136 (3.9%), S535 (3.9%), T558/T559 (3.9%), S570 (2.7%), S126 (2.3%), T548/T549 (1.9%), T394 (0.4%), and S526 (0.4%; Supplemental Table 1). Unfortunately, the peptide encompassing S600 was not recovered in the analysis (Supplemental Table 1), so phosphorylation of this residue cannot be assessed. These results suggest that ERK2-treated Drp1 is efficiently phosphorylated on S579, with minor phosphorylation on other residues. The presence of non-phospho-S579 peptides in the ERK2-treated sample (Supplemental Table 1) suggests that less than 100% of the Drp1 is phosphorylated, but this technique does not allow absolute quantification of phosphorylation percentage.

Similar to its phosphomimetic analogue, S579-phosphorylated Drp1 (P-S579-Drp1) is not stimulated by actin filaments (Figure 4D). In actin binding assays, P-S579-Drp1 displays an approximate two-fold decrease in maximal actin binding relative to Drp1-mock, while maintaining a similar affinity (Figure 4E; Supplemental Figure S3), similar to the S579D mutant. CL-containing vesicles only weakly stimulate P-S579-Drp1 (Figure 4F), which is a comparatively greater effect than that of the phosphomimetic. Similar to Drp1-S579D, P-S579-Drp1 is stimulated by Mff or by MiD49 oligomers to a lesser extent than Drp1-WT (Figure 4, G and H). Interestingly, the synergy of Mff with actin filaments is strongly reduced for Drp1-S579D (Figure 4I) while the synergy between Mff and MiD49 oligomers is maintained (Figure 4J).

A recent publication reports that phosphorylation at the S600 position can stimulate S579 phosphorylation in some cases, and this doubly phosphorylated Drp1 leads to increased mitochondrial fragmentation (Valera-Alberni *et al.*, 2021). We therefore tested whether doubly phosphorylated Drp1 displays different properties to either singly phosphorylated protein. For these experiments, we phosphorylated Drp1-S600D on S579 using Erk2, resulting in a similar gel shift as Drp1-phosphoS579 (Figure 5A) and similarly high spectral counts for phosphoS579 by phosphor-proteomics (Supplemental Table 1). As with Erk2-phosphorylated Drp1-WT, Drp1-phosphoS579/S600D is not activated by actin filaments or CL (Figure 5, B and C), and displays reduced activation by Mff (Figure 5D). Interestingly, Drp1-phosphoS579/S600D displays no activation by MiD49 oligomers (Figure 5E), and no synergistic effect of actin or MiD49 oligomers on Mff activation (Figure 5, F and G).

The Drp1 protein used thus far (isoform 3) contains none of the possible alternately spliced inserts identified for mammalian Drp1. While isoform 3 predominates in some cell types, it is a minor isoform in others, and the other splice variants also make up an appreciable percentage of total Drp1 in most cells and tissues (Strack *et al.*, 2013; Itoh *et al.*, 2018). In particular, the isoform containing all splice inserts (isoform 6) is uniquely expressed in brain (Itoh *et al.*, 2018). We therefore tested whether isoform 6 behaves similarly to isoform 3 in response to Erk2 phosphorylation. Treatment of isoform 6 with Erk2 results in decreased mobility on SDS–PAGE (Figure 6A), suggesting successful phosphorylation on S629 (equivalent to S579 in isoform 3). Similar to isoform 3, P-S629-Drp1(i6) is not activated by actin filaments (Figure 6B). In addition, Mff and MiD49 stimulate P-S629-Drp1(i6) to a lesser extent than nonphosphorylated Drp1 (Figure 6, C and D). These results suggest that the presence of the three splice inserts do not alter Drp1's response to phosphorylation on the canonical "activating" site.

Taken together, the results in this section show that Drp1-phosS579 possesses similar properties to the phosphomimetic S579D mutant in its reduced stimulation by all tested activators. In fact, Drp1-phosS579 displays less stimulation by CL than Drp1-S579D, and displays no synergy between actin and Mff.

Drp1-S579D does not stimulate actin-mediated activation of Drp1-WT

In a cellular context, it is likely that only a fraction of Drp1 is phosphorylated, even under conditions of cell activation. Therefore, we wished to test the effect of S579- and S600-phosphorylated Drp1 on nonphosphorylated Drp1. Our reasoning was as follows: if GTPase activation is a consequence of interaction between two neighboring GTPase domains, heteromeric assemblies between phosphorylated and nonphosphorylated Drp1 might have effects on GTPase activation.

The ability of the S579D to bind actin without stimulation of its GTPase activities allowed us to test the effects of Drp1-S579D on actin-mediated activation of Drp1-WT GTPase activity. We used GFP-tagged Drp1 as the WT version of Drp1, to distinguish between WT and mutant proteins in cosedimentation assays. In previous studies, we found that GFP-Drp1 displayed similar activity to un-tagged Drp1 (Hatch *et al.*, 2016; Liu *et al.*, 2021).

We varied percentages of Drp1-S579D and GFP-Drp1-WT, while maintaining a constant total Drp1 concentration, to assess effects on actin binding and actin-stimulated GTPase activity by the WT construct. In these experiments, we used concentrations of total Drp1 (1.3 μM) and actin (1 μM) that result in subsaturating Drp1 on actin. There is a linear increase in the percent GFP-Drp1 bound as the ratio of GFP-Drp1-WT:Drp1-S579D increases (Figure 7, A and B), suggesting no effects of Drp1-S579D on Drp1-WT binding to filaments. Interestingly, there is a nonlinear increase in actin-stimulated GTPase activity when GFP-Drp1-WT is titrated into Drp1-S579D, whereby no increase in GTPase activity is observed until 40% GFP-Drp1-WT is present (Figure 7C). A similar nonlinear effect of Drp1-S579D occurs when untagged Drp1-WT is used (Figure 7D), indicating that the GFP-tag is not the source of the effect. This nonlinear

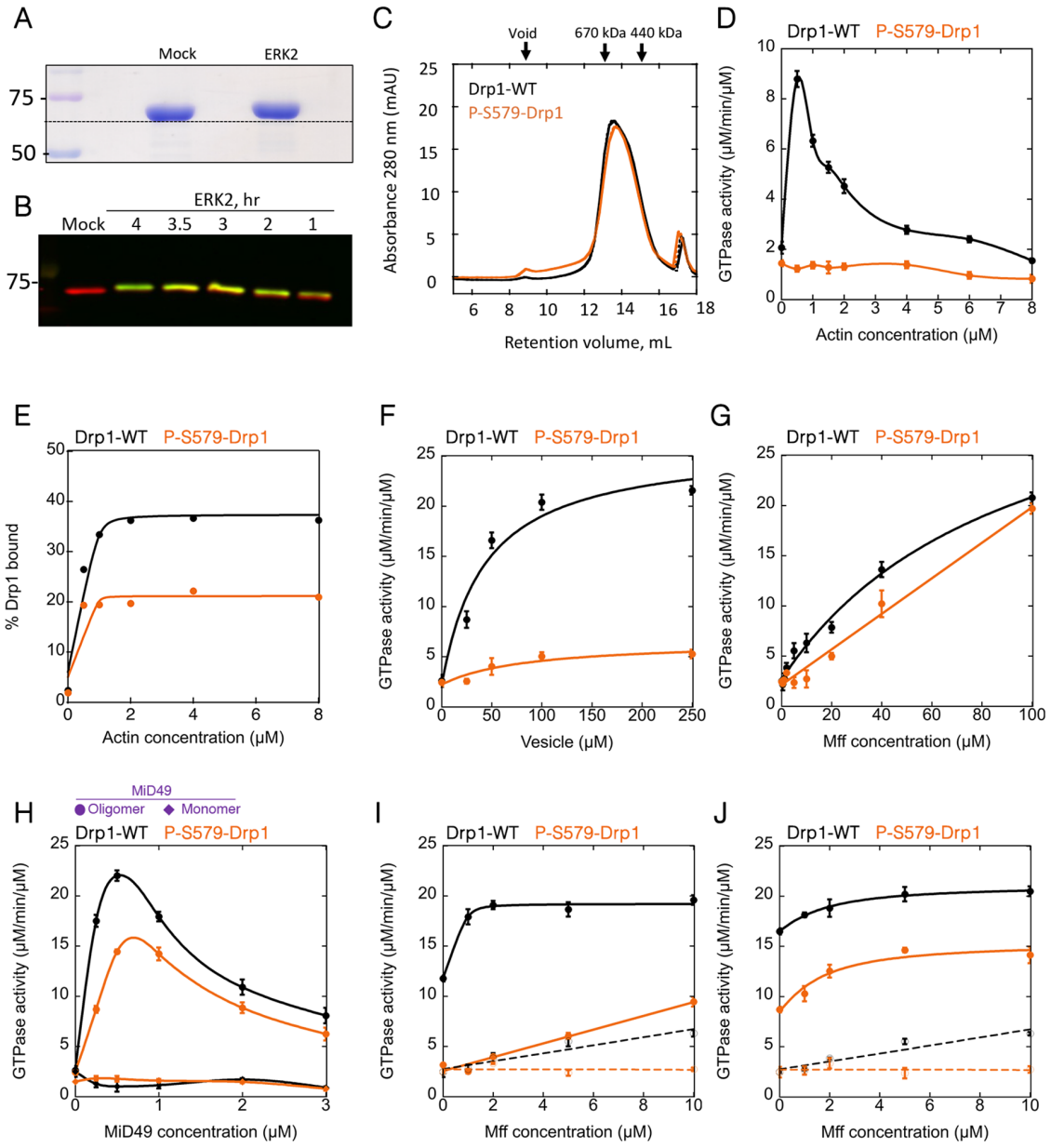

FIGURE 4: Effects of Phospho-S579-Drp1 on actin binding and GTPase stimulation by actin, Mff, and MiD49. In all graphs, Drp1-WT and P-S579-Drp1 in black and orange, respectively. All GTPase assays contain 0.75 μM Drp1. (A) Coomassie-stained SDS–PAGE of Drp1 from either mock phosphorylation or ERK2 phosphorylation reactions (4 h). 2 μg Drp1 on gel. Positions of size standards (in kDa) on left. (B) Western blot showing anti-Drp1 (red) and anti-phospho-S579-Drp1 (green) at varying times after ERK2 treatment. (C) Superose 6 gel filtration profiles of WT and P-S579-Drp1. At top are peak elution positions for two standards (thyroglobulin [670 kDa] and ferritin [440 kDa]) as well as the void volume position. (D) GTPase assays containing Drp1 that was preincubated with the indicated concentration of actin filaments for 5 min before GTP addition. Activity expressed as μM phosphate released per min per μM Drp1. (E) Graph of % Drp1 bound versus actin concentration, from cosedimentation assays at 65 mM NaCl. Raw data in Supplemental Figure S2. (F) GTPase assays containing Drp1 that was preincubated with the indicated concentration of CL-containing vesicles (μM total lipid, vesicles contain 40% DOPC, 35% DOPE, and 25% CL) for 5 min before GTP addition. (G) Comparison of WT and P-S579-Drp1 GTPase activities in the presence of the indicated concentration of Mff for 5 min before GTP addition. (H) Comparison of WT and P-S579-Drp1 GTPase activities in the presence of the indicated concentration of MiD49 monomer (diamond) or MiD49 oligomer (circle) for 5 min before GTP addition. (I) Comparison of WT and P-S579-Drp1 GTPase activities in the presence of 0.5-μm actin filaments and the indicated concentration of Mff for 5 min before GTP addition. Values for Mff alone are indicated by open circles and dashed lines, while values for Mff/actin are indicated by closed circles and solid lines. (J) Comparison of WT and P-S579-Drp1 GTPase activities in the presence of 0.25 μM MiD49 oligomer and the indicated concentration of Mff for 5 min before GTP addition. Values for Mff alone are indicated by open circles and dashed lines, while values for Mff/MiD49 are indicated by closed circles and solid lines. Error bars represent mean ± S.D. ($n = 3$).

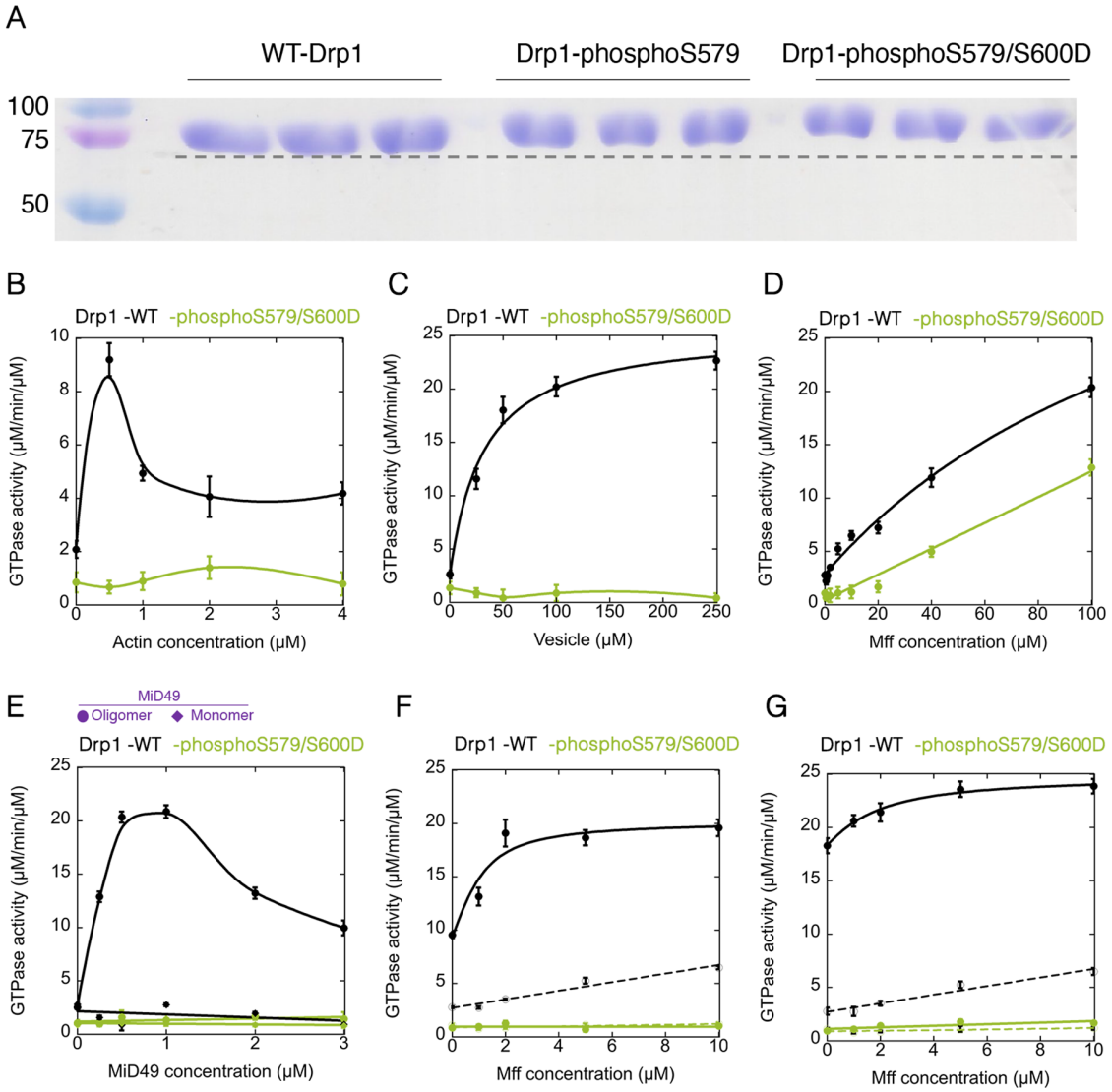

FIGURE 5: Effects of Drp1-phosphoS579/S600D on GTPase stimulation. In all graphs, Drp1-WT and Drp1-phosphoS579/S600D in black and green, respectively. All GTPase assays contain 0.75 μM Drp1. (A) Coomassie-stained SDS–PAGE of Drp1 from either Drp1- mock phosphorylation, Drp1- ERK2 phosphorylation, or Drp1-S600D- ERK2 phosphorylation reactions (4 h). 2 μg Drp1 on gel. Positions of size standards (in kDa) on left. (B) GTPase assays containing Drp1 that was preincubated with the indicated concentration of actin filaments for 5 min before GTP addition. Activity expressed as μM phosphate released per minute per μM Drp1. (C) GTPase assays containing Drp1 that was preincubated with the indicated concentration of CL-containing vesicles (40% DOPC, 35% DOPE, and 25% CL) for 5 min before GTP addition. (D) Comparison of Drp1-WT and Drp1-phosphoS579/S600D GTPase activities in the presence of the indicated concentration of Mff for 5 min before GTP addition. (E) Comparison of Drp1-WT and Drp1-phosphoS579/S600D activities in the presence of the indicated concentration of MiD49 monomer (diamond) or MiD49 oligomer (circle) for 5 min before GTP addition. (F) Comparison of Drp1-WT and Drp1-phosphoS579/S600D GTPase activities in the presence of 0.5 μm actin filaments and the indicated concentration of Mff for 5 min before GTP addition. Values for Mff alone are indicated by open circles and dashed lines, while values for Mff/actin are indicated by closed circles and solid lines. (G) Comparison of Drp1-WT and Drp1-phosphoS579/S600D activities in the presence of 0.25 μM MiD49 oligomer and the indicated concentration of Mff for 5 min before GTP addition. Values for Mff alone are indicated by open circles and dashed lines, while values for Mff/MiD49 are indicated by closed circles and solid lines. Error bars represent mean ± S.D. ($n = 3$).

effect of Drp1-S579D on actin-activated Drp1-WT GTPase activity suggests that the S579D mutant slightly inhibits Drp1-WT activation when heteromerically bound to actin.

We tested an additional mutant, Drp1-K38A, for effects on Drp1-WT activity under activating conditions. This mutant is widely used as a dominant-negative in cellular experiments. An equivalent mutant in dynamin 1 is also a dominant-negative in cells, but causes increased oligomerization of the wild-type protein (Warnock *et al.*, 1996). As expected, Drp1-K38A displays no GTP hydrolysis in the absence or presence of actin filaments (Figure 8A), while binding actin filaments with similar properties to Drp1-WT (Figure 8, B and C).

The absence of all GTPase activity for Drp1-K38A allowed us to test its effect on the specific activity of Drp1-WT directly, when the two are bound to actin filaments. Interestingly, Drp1-K38A has a

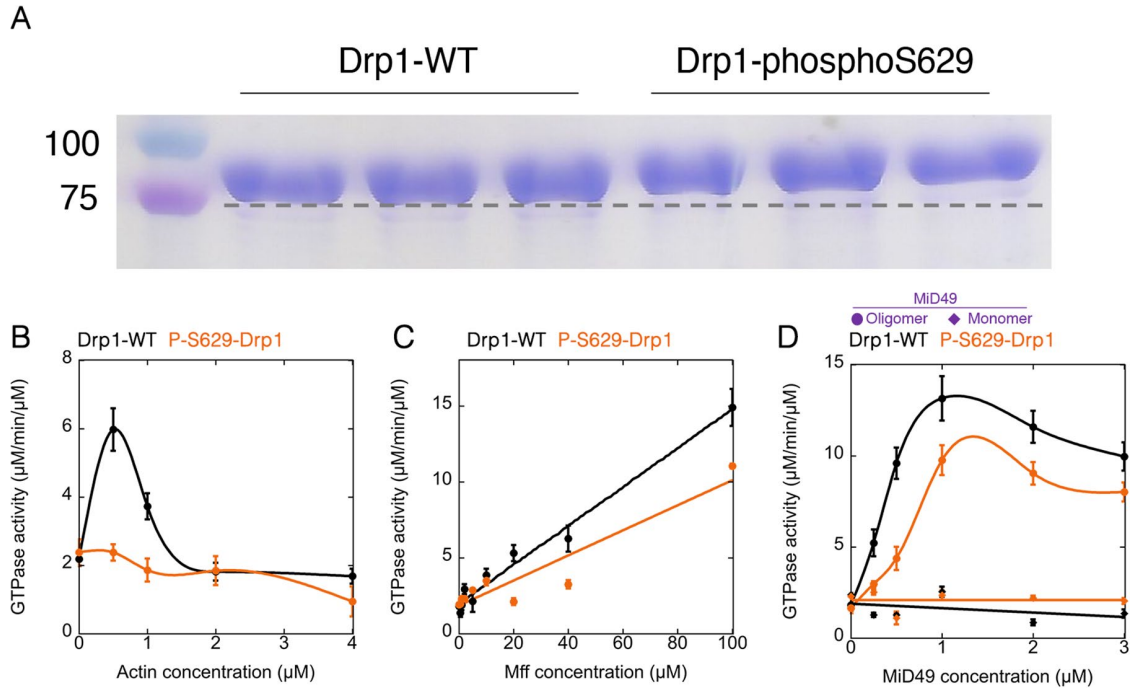

FIGURE 6: Effects of Erk2 phosphorylation on GTPase activity of Drp1 isoform 6. In all graphs, Drp1-WT and Drp1-phosphoS629 in black and orange, respectively. All GTPase assays contain 0.75 μM Drp1. (A) Coomassie-stained SDS–PAGE of Drp1 isoform 6 from either Drp1- mock phosphorylation or Drp1- ERK2 phosphorylation (4 h). 2 μg Drp1 on gel. Positions of size standards (in kDa) on left. (B) GTPase assays containing Drp1 that was preincubated with the indicated concentration of actin filaments for 5 min before GTP addition. Activity expressed as μM phosphate released per minute per μM Drp1. (C) Comparison of Drp1-WT and P-S629-Drp1 GTPase activities in the presence of the indicated concentration of Mff for 5 min before GTP addition. (E) Comparison of Drp1-WT and P-S629-Drp1 activities in the presence of the indicated concentration of MiD49 monomer (diamonds) or MiD49 oligomer (circles) for 5 min before GTP addition. Error bars represent mean ± S.D. ($n = 3$).

significant stimulatory effect on actin-activated GTPase activity for Drp1-WT in these assays. The maximum effect occurs at 30–40% Drp1-K38A, where Drp1-WT specific activity is over three-fold higher than for 100% Drp1-WT (Figure 8D). We also compared GTPase activity of varying ratios of WT and K38A mutants with no actin present. In this case, K38A has an even more dramatic effect, with an 80:20 ratio of K38A:WT having 10-fold higher specific activity than 100% Drp1 (Figure 8E). A similar effect has previously been observed for dynamin-1 (Warnock *et al.*, 1996).

To verify that the stimulatory effect of Drp1-K38A on Drp1-WT is due to heterooligomerization, we utilized the Drp1 dimer mutant (Drp1-DM) in place of Drp1-WT. Drp1-DM has similar basal GTPase activity to Drp1-WT (Fröhlich *et al.*, 2013), but remains dimeric at all concentrations tested and does not form a sedimentable species in the presence of GMP-PCP (Hatch *et al.*, 2016). As the percentage of Drp1-DM increases relative to Drp1-K38A, there is a linear increase in GTPase activity and no increase in specific activity (Figure 8F). We conclude that the stimulatory effect of Drp1-K38A on Drp1-WT GTPase activity is due to heterooligomerization effects.

These results suggest that Drp1-S579D reduces the activity of Drp1-WT when both are bound to actin filaments. In contrast, the GTPase activity of Drp1-WT is increased by the proximity of the catalytically inactive Drp1-K38A, either when bound to actin filaments or free in solution.

DISCUSSION

In this study, we have tested the effects of two phosphomimetic mutants on Drp1 activity. The S579D mutant is widely thought to be stimulatory to Drp1 activity in cells (Taguchi *et al.*, 2007; Qi *et al.*, 2011; Yu *et al.*, 2011; Strack *et al.*, 2013; Kashatus *et al.*, 2015; Serasinghe *et al.*, 2015; Xu *et al.*, 2016; Brand *et al.*, 2018; Han *et al.*, 2020), while the S600D mutant has been shown to be inhibitory in most cellular studies (Chang and Blackstone, 2007; Cribbs and Strack, 2007; Cereghetti *et al.*, 2008; Wikstrom *et al.*, 2013), but stimulatory in others (Han *et al.*, 2008; Wang *et al.*, 2012; Jhun *et al.*, 2018; Galvan *et al.*, 2019). Both phosphomimetic mutants display decreased oligomerization in a GTP-free state, but oligomerize in the presence of GMP-PCP. Both phosphomimetic mutants display low GTPase stimulation by actin filaments, and reduced stimulation by CL or the Drp1 receptors Mff and MiD49. Drp1 phosphorylated in vitro on S579 displays similar attributes, with its CL-stimulated GTPase activity being even less than for its corresponding phosphomimetic. When mixed with Drp1-WT on actin filaments, Drp1-S579D decreases the actin-stimulated activity of Drp1-WT.

The most striking aspect of these results is that phosphorylation at the S579 site, which has been associated with increased Drp1 activity in cellular studies, causes a decrease in activator-stimulated GTP hydrolysis, a fundamental readout of biochemical Drp1 activity. One possible reason for this apparent contradiction is that the Drp1 isoforms used here: isoform 3, which contains none of the alternately spliced exons; and isoform 6, which contains all three exons (Figure 1), do not display activation by S579 phosphorylation while other isoforms do. In the most comprehensive assessments to-date of Drp1 isoform abundance at the protein (Strack *et al.*, 2013) and mRNA level (Itoh *et al.*, 2018), most cell and tissue types contain a mix of isoforms, with isoform 3 being the most abundant in some

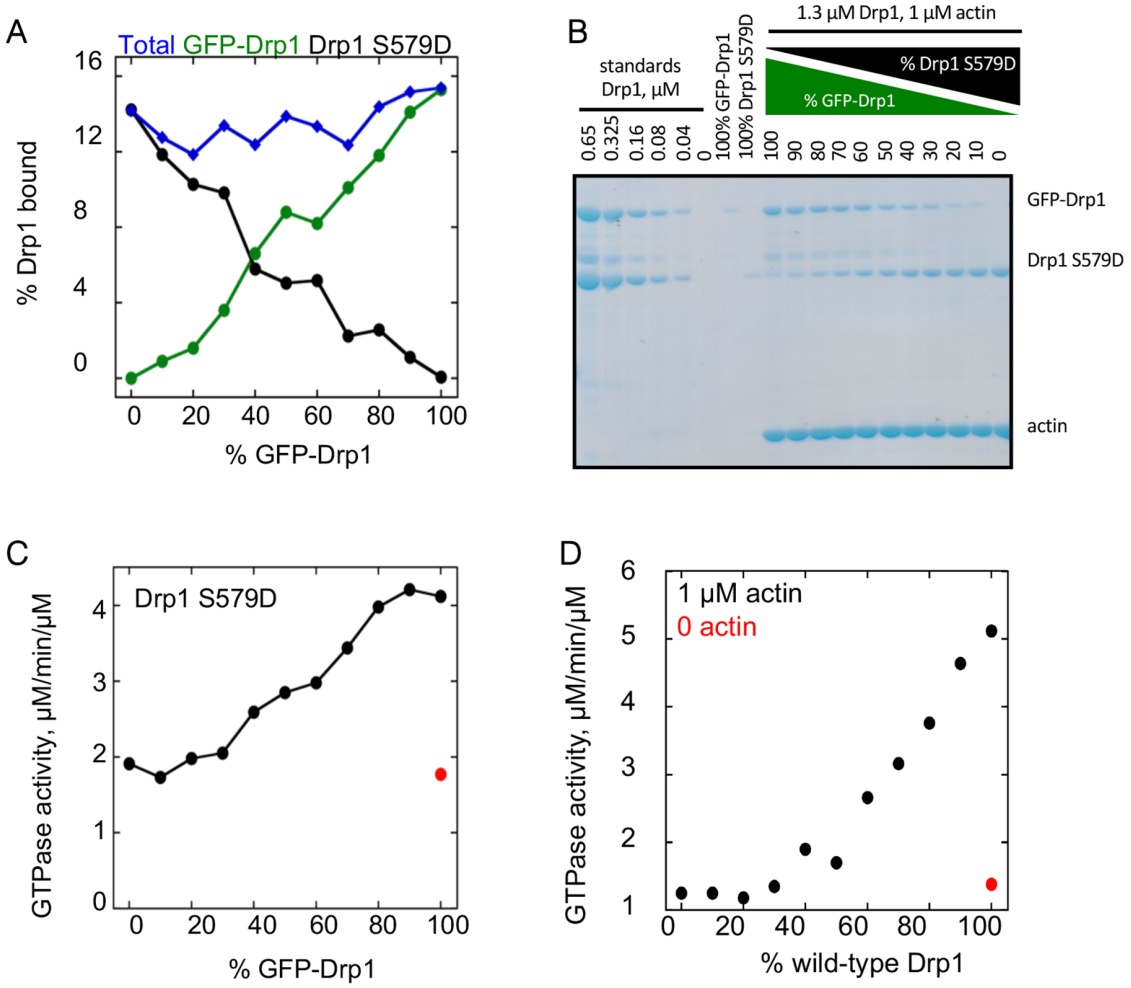

FIGURE 7: Drp1 phosphomimetic mutants reduce the ability of actin filaments to activate wild-type Drp1. In all panels, the actin filament concentration is constant at 1 μM, and the total Drp1 concentration (combination of GFP-Drp1 and phosphomimetic mutant Drp1 without GFP) is constant at 1.3 μM. (A) Graph of Drp1 binding to actin filaments with varying ratios of GFP-Drp1-WT:Drp1-S579D. (B) Corresponding Coomassie gels for binding assays quantified in panel A. (C) GTPase activity of Drp1 at varying ratios of GFP-Drp1-WT:Drp1-S579D in the presence of actin filaments. Red point represents GTPase activity of GFP-Drp1-WT in the absence of actin filaments. (D) GTPase activity of Drp1 (without the GFP tag) at varying ratios of Drp1-WT:Drp1-S579D in the presence of actin filaments. Red point represents GTPase activity of Drp1-WT in the absence of actin filaments.

(but not all) cell lines. Nonetheless, other isoforms represent a significant proportion of total Drp1. Considering that two alternatively spliced exons lie near the S579 site, additional studies are needed to test isoform-specific effects of phosphorylation.

Another possibility is that the positive effect of S579 phosphorylation depends on additional factors. For instance, S579 phosphorylation might result in recruitment of a factor that is stimulatory to Drp1 oligomerization, GTPase activity, or ability to constrict membranes. It is unclear what such a factor might be, but one possibility is a member of the nucleotide diphosphate kinase (NDPK) family that can catalyze GTP synthesis from guanosine diphosphate (GDP) and adenosine triphosphate (ATP). Cytosolic NDPK family members NME1 and NME2 have been shown to increase activity of dynamin1 and dynamin2, while mitochondrial NME4 increases activity of the mitochondrial inner membrane dynamin Opa1 under conditions of low GTP (Boissan *et al.*, 2014). Physical interaction between these NDPKs and their respective dynamin proteins might raise the local concentration of GTP, increasing GTPase activity. There is evidence that another NDPK, NME3 enriches on peroxisomes and mitochondria, and might work with Drp1 in a similar manner (Honsho *et al.*, 2020; Abe *et al.*, 2023). However, this NDPK has also been implicated in mitochondrial fusion (Chen *et al.*, 2019; Ikeda *et al.*, 2023). A second possibility is influence of Drp1 phosphorylation on inner mitochondrial membrane fission, through factors like the recently identified Mdi1/Atg44 (Connor *et al.*, 2023). However, Mdi1 does not have clear mammalian homologues. In addition, inner mitochondrial membrane dynamics appear to precede outer mitochondrial membrane dynamics where examined (Cho *et al.*, 2017; Chakrabarti *et al.*, 2018).

Our results also provide information as to Drp1's interaction with actin filaments. Both phosphomimetic mutations, as well as S579 in vitro phosphorylation, eliminate actin-activated GTPase activity. This effect suggests that the VD is involved in the actin interaction. Interestingly, actin still seems to synergize with Mff for activation of the phosphomimetics, suggesting that the important feature for this synergy is actin binding, not the activation that actin alone causes for Drp1.

It should be noted that, while the phosphomimetic S579D mutant largely displays similar properties to S579-phosphorylated

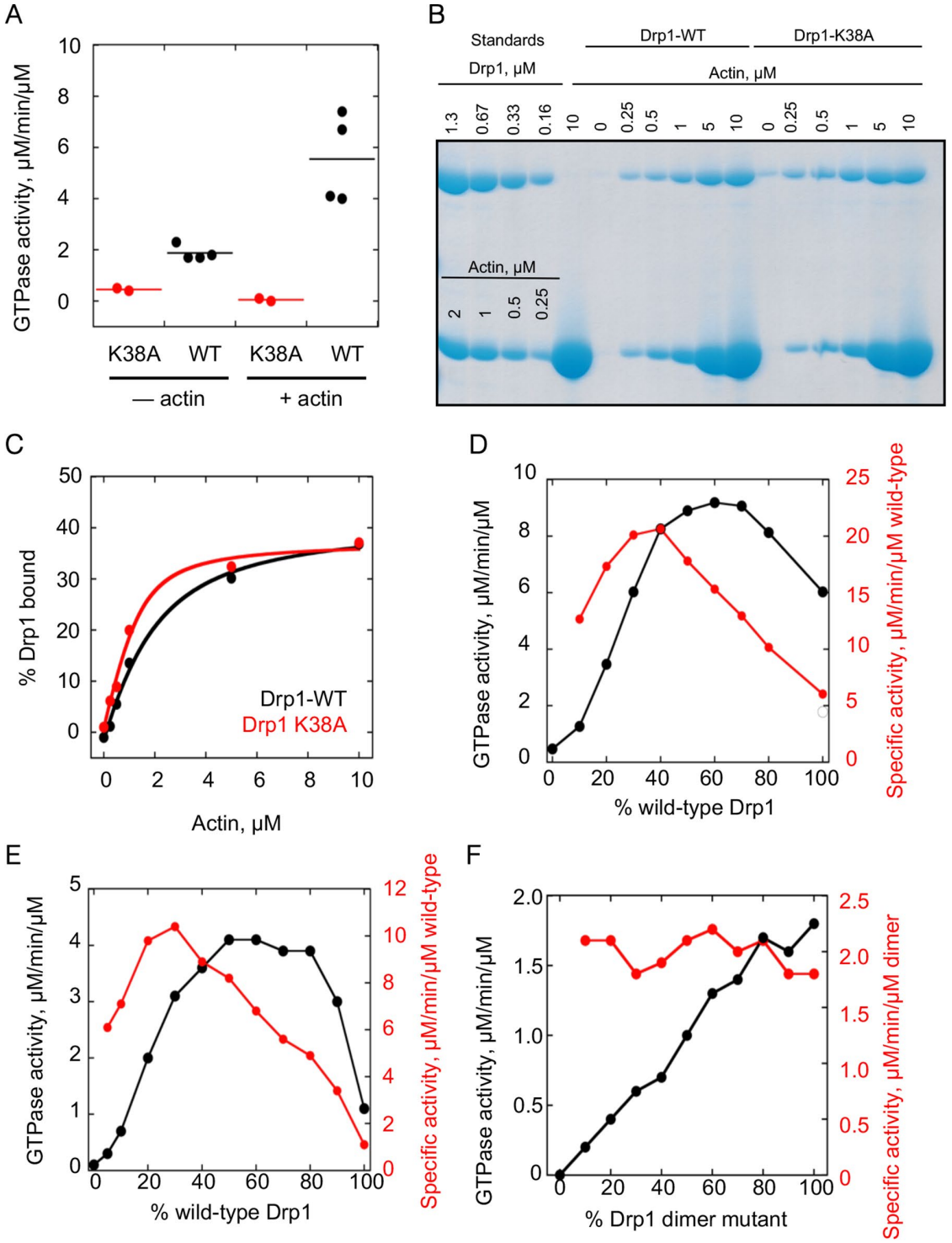

FIGURE 8: Drp1-K38A mutant stimulates the GTPase activity of Drp1-WT. (A) GTPase activity of Drp1-WT or Drp1-K38A (1.3 μM) in the presence or absence of actin filaments (1 μM). (B) Coomassie-stained SDS–PAGE of Drp1/actin cosedimentation at 65 mM NaCl, with 1.3 μM Drp1-WT or Drp1-K38A and varying actin. Standards of known μM amounts of Drp1-WT and actin on left, pellets from sedimentation assays on right. (C) Graph of percent Drp1 in the pellet for Drp1-WT and Drp1-K38A as a function of actin concentration. (D) GTPase activity of Drp1 at varying ratios of Drp1-WT:Drp1-K38A (1.3 μM total Drp1) in the presence of actin filaments (1 μM). Black line denotes total Drp1 specific activity (factoring both WT and K38A mutant) while red line denotes specific activity of Drp1-WT. (E) GTPase activity of Drp1 at varying ratios of Drp1-WT:Drp1-K38A (1.3 μM total Drp1) in the absence of actin filaments. Black line and red lines as described in panel D. (F) GTPase activity of Drp1 at varying ratios of Drp1-DM:Drp1-K38A (1.3 μM total Drp1) in the presence of actin filaments (1 μM). Black line denotes total Drp1 specific activity (factoring both Drp1-DM and K38A mutant) while red line denotes specific activity of Drp1-DM. DM, dimer mutant.

Drp1, the effects of phosphorylation are generally more pronounced. In particular, activation by CL-containing vesicles, as well as the synergy between actin and Mff, is practically eliminated for Drp1-phosphoS579, whereas it is partially inhibited for Drp1-S579D.

It is important to point out aspects of our study that merit more testing. One aspect is the effects of phosphorylation on all physiologically-expressed Drp1 isoforms (mentioned earlier in the Discussion). Another aspect is the effect of Drp1 phosphorylation on its interaction with MiD51, because we only test MiD49 here. While our recent results suggest that MiD49 and MiD51 respond similarly to their activator (fatty acyl-CoA; Liu *et al.*, 2023), it is possible that MiD51 could interact differentially with phosphorylated Drp1. In addition, the issue of how phosphorylation or the phosphomimetic mutants influence binding to specific activators must be examined in more detail, because the experiments conducted here (cosedimentation) were only carried out for a subset of activators (actin filaments and Mff), and in the case of Mff were not conducted in a manner that allows determination of interaction affinity. Finally, detailed structural analysis (such as by electron microscopy) of Drp1 conformation when in the GTP-bound state or on CL-containing membranes, actin filaments, or MiD49 oligomers would provide information as to the manner in which S579 and/or S600 phosphorylation affect Drp1 packing during oligomerization or activation.

Finally, the inhibitory effect of Drp1-S579D on WT Drp1 GTPase activity is likely due to the decreased oligomerization of the mutant, which decreases the interactions between G domains necessary for GTPase activation. In contrast, the K38A mutation might activate WT Drp1 by stabilization of the oligomeric state. A similar effect of the equivalent mutation in dynamin-1, K44A, was described many years ago (Warnock *et al.*, 1996). These results emphasize the effect of oligomerization on Drp1 activity, with mechanisms that increase oligomerization being likely to increase GTPase activity.

MATERIALS AND METHODS

Request a protocol through *Bio-protocol*.

Methods

Plasmids. For bacterial expression, full-length of human DRP1 isoform 3 (NP_055681.2, UniProt ID O00429-4), Drp1 isoform 6 (UniProt ID O00429-6), truncated human MFF isoform 4 (UniProt ID Q9GZY8-4; MFF-ΔTM), and MiD49Δ1-124 (mouse amino acids 125-454, UniProt ID Q5NCS9) have been described previously (Hatch *et al.*, 2016; Osellame *et al.*, 2016; Liu *et al.*, 2023). Quick Change mutagenesis was performed to make Drp1 mutants K38A, S579D, S600D, and Drp1 dimer mutant (Drp1-DM; Fröhlich *et al.*, 2013; Hatch *et al.*, 2016). For GFP-Drp1, Drp1 isoform 3 is expressed with an N-terminal eGFP tag (A206K mutant to reduce GFP dimerization) using the pET-16b vector (Novagen, EMD Millipore, Billerica MA), as previously described (Hatch *et al.*, 2016). Briefly, the expressed construct contains the following sequence elements (from N- to C-terminus): FLAG tag, 2xStrep affinity tag separated by a Gly-Ser linker, HRV3C protease site, GFP A206K mutant, Drp1 isoform 3. During purification, HRV3C cleavage results in retention of only the GFP and Drp1 sequences in the construct. The amino acid sequences of the construct precleavage and postcleavage are given in Supplemental Figure S4. A previous report found that bacterially-expressed Drp1 that was N-terminally GFP-tagged was significantly compromised in terms of GTPase activity (Montecinos-Franjola *et al.*, 2020). Our GFP-fusion construct does not display reduced GTPase activity, either in this work or in our previous work (Hatch *et al.*, 2016; Liu *et al.*, 2021). Possible reasons for differences between the constructs are: use of a 6His tag and Ni-NTA chromatography in (Montecinos-Franjola *et al.*, 2020) versus 2Strep tag purification in this study, retention of the N-terminal 6His tag on the construct used in (Montecinos-Franjola *et al.*, 2020), differences in the length/sequence of the linker between GFP and Drp1 (our linker shown in Supplemental Figure S4, nature of the linker in is [Montecinos-Franjola *et al.*, 2020] unclear), or differences in other purification/storage techniques.

Protein expression, purification. All Drp1 constructs were expressed and purified as previously described with modifications (Hatch *et al.*, 2016). Briefly, DRP1 construct was expressed in One Shot BL21 Star (DE3) *Escherichia coli* in LB broth, induced by isopropyl-β-D-thiogalactoside (IPTG) at 16°C for 16 h when OD600 reached to 1.5. Cell pellets were resuspended in lysis buffer (100 mM Tris-Cl, pH 8.0, 500 mM NaCl, 1 mM dithiothreitol [DTT], 1 mM Ethylenediaminetetraacetic acid [EDTA], 2 μg/ml leupeptin, 10 μg/ml aprotinin, 2 μg/ml pepstatin A, 2 mM benzamidine, 1 μg/ml ALLN, and 1 μg/ml calpeptin) and lysed using a high-pressure homogenizer. The lysate was cleared by centrifugation at 40,000 rpm in Ti-45 rotor for 1 h at 4°C. Avidin (20 μg/ml; PI-21128; Thermo Fisher Scientific, Waltham, MA) was added to the supernatant, and then was loaded onto Strep-Tactin Superflow resin (2-1206-025; IBA, Göttingen, Germany) by gravity flow. The column was washed with 20 column volumes (CV) of lysis buffer without protease inhibitors. To elute DRP1, 0.01 mg/ml HRV3C protease in lysis buffer without protease inhibitors was added for 16 h at 4°C. The Strep-Tactin Superflow eluate was further purified by size exclusion chromatography on Superdex200 with DRP1-S200 buffer (20 mM HEPES pH 7.5, 150 mM KCl, 2 mM $MgCl_2$, 1 mM DTT, 0.5 mM EGTA), spin concentrated, frozen in liquid nitrogen, and stored at –80°C.

MFF-ΔTM was expressed in Rosetta™2 BL21-(DE3) *Escherichia coli* (71400; EMD Millipore Corporation, Burlington, MA) in LB broth, induced by 1M IPTG at 30°C for 4 h when OD600 reached to 1.5. Cell pellets were resuspended in lysis buffer (50 mM Tris-HCl, pH 7.5, 500 mM NaCl, 20 mM imidazole, pH 7.5, 1 mM DTT, 1 mM EDTA, 2 μg/ml leupeptin, 10 μg/ml aprotinin, 2 μg/ml pepstatin A, 2 mM benzamidine, 1 μg/ml ALLN, and 1 μg/ml calpeptin) and lysed using M-110 microfluidizer processor. The lysate was cleared by centrifugation at 40, 000 rpm in Ti45 for 40 min at 4°C, the supernatant was saved. Affinity capture was performed using FPLC and a HiTrap IMAC column (17-5248-01, GE Healthcare, Chicago, IL) equilibrated with IMAC-A buffer (50 mM Tris-HCl pH 7.5, 0.1 M NaCl, 20 mM imidazole). Cleared lysate was loaded onto the column with a rate of 3 ml/min and washed to baseline with IMAC-A. MFF was eluted from the column with gradient step washes by IMAC-B buffer (50 mM Tris-HCl pH 7.5, 0.1 M NaCl, 500 mM imidazole): step1 10% IMAC-B for 5CV, step2 20% IMAC-B for 5CV, step3 100% for 5CV. Fractions from step3 were pooled and diluted 10-fold in ion exchange (IEX)-A buffer (50 mM Tris-HCl pH 7.5, 1 mM DTT). Diluted fractions were loaded onto a HiTrap Q anion exchange column (54816, EMD Millipore Corporation, Burlington, MA). The column was washed to baseline with IEX-A and MFF was eluted by IEX-B buffer (50 mM Tris-HCl pH 7.5, 1 M NaCl, 1 mM DTT) with a step gradient: step1 10% 5CV, linear 10-50% 30CV followed by linear 50-100% 5CV. Peak MFF fractions were concentrated by reloading onto the HiTrap IMAC column and eluted with 100% IMAC-B step wash. MFF fractions were pooled and further purified by size exclusion chromatography on Superdex200 with S200 buffer (20 mM HEPES, pH 7.4; 2 mM $MgCl_2$, 0.5 mM EGTA, 65 mM KCl, 1 mM DTT), spin concentrated (UFC903024, EMD

Millipore Corporation, Burlington, MA), aliquots were frozen in liquid nitrogen, and stored at −80°C.

MiD49 was expressed in One Shot BL21 Star (DE3) *Escherichia coli* (C6010-03; Life Technologies, Carlsbad, CA) in LB broth, induced by IPTG at 16°C for 16 h when OD600 reached 1.5. Cell pellets were resuspended in MiD lysis buffer (25 mM 4-[2-hydroxyethyl]-1-piperazineethanesulfonic acid [HEPES], pH 7.4, 500 mM NaCl, 1 mM dithiothreitol [DTT], 2 μg/ml leupeptin, 10 μg/ml aprotinin, 2 μg/ml pepstatin A, 2 mM benzamidine, 1 μg/ml calpain inhibitor I [ALLN], and 1 μg/ml calpeptin) and lysed using a high-pressure homogenizer (M-110L Microfluidizer Processor; Microfluidics, Newton, MA). The lysate was cleared by centrifugation at 40,000 rpm (type 45 Ti rotor; Beckman, Brea, CA) for 1 h at 4°C and then was loaded onto Pierce Glutathione Agarose (16101; Thermo Fisher Scientific) by gravity flow. The column was washed with 20 CV of lysis buffer without protease inhibitors. To elute MiD49/51, 1 unit/μL thrombin (T4648, Sigma-Aldrich) or 0.01 mg/ml HRV3C protease in lysis buffer without protease inhibitors was added for 16 h at 4°C. The protein eluate was captured by HiTrap IMAC column (17-5248-01, GE Healthcare, Chicago, IL) and eluted by IMAC-B buffer (50 mM Tris-HCl pH 7.5, 0.1 M NaCl, 500 mM imidazole). The His-trap protein eluate was further purified by size exclusion chromatography on Superdex200 (GE Biosciences, Piscataway, NJ) with S200 buffer (20 mM HEPES, pH 7.4, 65 mM KCl, 2 mM $MgCl_2$, 1 mM DTT, 0.5 mM ethylene glycol tetraacetic acid [EGTA]), spin concentrated (UFC903024, EMD Millipore Corporation, Burlington, MA), frozen in liquid nitrogen, and stored at −80°C.

Rabbit skeletal muscle actin was extracted from acetone powder as previously described (Spudich and Watt, 1971), and further gel-filtered on Superdex 75 16/60 columns (GE Healthcare). Actin was stored in G buffer (2 mM Tris, pH 8.0, 0.5 mM DTT, 0.2 mM ATP, 0.1 mM $CaCl_2$, and 0.01% NaN_3) at 4°C.

In vitro phosphorylation of Drp1 by ERK2. For in vitro phosphorylation assay, 30 μM purified Drp1 or Drp1-S600D was incubated with 100 nM ERK2 kinase (Thermo Fisher Scientific PV3313) at 30°C for 4 h. Reaction was conducted in 25 mM HEPES, pH 7.4, 150 mM KCl, 10 mM $MgCl_2$, 2 mM DTT, 1 mM ethylene glycol tetraacetic acid [EGTA]), 1% Thesit. Phosphorylated Drp1 was further purified by size exclusion chromatography on Superdex200 with S200 buffer (20 mM HEPES, pH 7.4; 2 mM $MgCl_2$, 0.5 mM EGTA, 65 mM KCl, 1 mM DTT), spin concentrated (UFC903024, EMD Millipore Corporation, Burlington, MA), aliquots were frozen in liquid nitrogen, and stored at −80°C.

Phospho-Drp1 analysis by mass spectrometry. In vitro phosphorylated Drp1 were diluted in SDS–PAGE sample buffer and resolved by SDS–PAGE. Gels were stained with Coomassie blue staining. Bands were excised from the gel (2 μg Drp1) and analyzed for phosphorylated peptides by the IDEA National Resource for Quantitative Proteomics (Little Rock, Arkansas, USA). Three independent samples were analyzed for untreated Drp1 isoform 3, ERK2-treated Drp1 isoform 3, and ERK2-treated Drp1 isoform 3 S600D mutant. Data were analyzed using Scaffold 5.3.0 (Proteome Software). Summary of the analysis is given in Supplemental Table 1. Briefly, between 92 and 95% coverage of the proteins was obtained. Spectral counts for phospho-S/T were obtained for ERK2-treated samples on the following residues percentage of overall phospho-counts for all samples): S579 (80%), T548/T549 (4.5%), S136 (4.3%), S535 (3.3%),T558/T559 (2.9%), S570 (2%), S126 (2%), T394 (0.4%), S526 (0.4%). The following serines/threonines were not covered for any of the nine samples, so assessment of their phosphorylation states cannot be determined: T96, S200, T282, and T288. Only one peptide containing S600 was identified for any of the nine samples (in untreated Drp1 isoform 3 sample 1) so S600 phosphorylation similarly was not able to be determined. The mass spectrometry proteomics data have been deposited to the ProteomeXchange Consortium via the PRIDE partner repository (Perez-Riverol *et al.*, 2022) with the dataset identifier PXD046824 and 10.6019/PXD046824.

Actin preparation for biochemical assays. For high-speed pelleting assay, actin filaments were polymerized from 20 μM monomers for 3 h at 23°C by addition of a 10× stock of polymerization buffer (200 mM HEPES, pH 7.4, 650 mM KCl, 10 mM $MgCl_2$, 10 mM EGTA) to a final 1× concentration, following established procedures (Harris and Higgs, 2006). For GTPase assay, actin monomers in G-buffer were incubated with AG1-X2 100–200 mesh anion exchange resin (Dowex; 1401241; Bio-Rad) at 4°C for 5 min to remove ATP, followed by low-speed centrifugation. 20 μM actin filaments were polymerized as described before. To maintain ionic strength across all samples, an actin blank was prepared in parallel using G-buffer in place of actin monomers and used to dilute actin filaments as needed for each sample. DRP1 was diluted in MEHD buffer (20 mM HEPES, pH 7.4, 2 mM $MgCl_2$, 0.5 mM EGTA, 1 mM DTT) to adjust the ionic strength to the same as S200 buffer before biochemical assays.

Size exclusion Chromatography assays. Drp1 and Dpr1-phosS579 oligomeric distribution was determined by Superose 6 increase 10/300 GL SEC column (GE Biosciences) in S200 buffer (20 mM HEPES, pH7.4, 65 mM KCl, 2 mM $MgCl_2$, 0.5 mM EGTA, 1 mM DTT). Protein at varying concentration was loaded onto the column in a total volume of 500 μl and gel-filtered with a flow rate of 0.4 ml/min.

MiD49 oligomer preparation. For in making MiD49 oligomer, 100μM purified MiD49Δ1-124 were incubated with 500μM Palmitoyl-CoA (Sigma-Aldrich, P9716) at 37°C for 1 h. Reaction was conducted in with S200 buffer (20 mM HEPES, pH 7.4; 2 mM $MgCl_2$, 0.5 mM EGTA, 65 mM KCl, 1 mM DTT). MiD49Δ1-124 mixture was further purified by size exclusion chromatography on Superdex200 with S200 buffer.

Liposome preparation. All lipids were purchased from Avanti Polar Lipids (Alabaster, AL). Liposomes were prepared by extrusion through polycarbonate membranes of 250 nm pore diameter. 0% CL liposome contained 65% DOPC (850375P, Avanti Polar lipid) and 35% DOPE (850725, Avanti Polar lipid). 25% CL liposome contained 40% DOPC, 35% DOPE, and 25% CL (840012C, Avanti Polar lipid).

GTPase assay. DRP1 (0.75 μM) was mixed with indicated concentrations of MiD49, MFF and/or actin filaments in S200 buffer. Sample were incubated at 37°C for 5 min. At this point, GTP was added to a final concentration of 500 μM to start the reaction at 37°C. Reactions were quenched at designated time points by mixing 15 μl sample with 5 μl of 125 mM EDTA in a clear, flat-bottomed, 96-well plate (Greiner, Monroe, NC). Six time points were acquired for all conditions, either in a 12-min time range, or in a 45-min time range depending on reaction speed. Released phosphate was determined by addition of 150 μl of malachite green solution as previously described (Hatch *et al.*, 2016) Absorbance at 650 nm was measured 15 min after malachite green solution incubation. GTP hydrolysis rates were determined by determining the slope of increase in phosphate concentration as a function of time in the linear phase of

the reaction. For reactions including mixtures of WT Drp1 and Drp1-K38A, total GTPase activity is calculated as a function of the μM concentration of total Drp1 (WT and K38A combined), whereas specific activity is calculated by using the μM concentration of WT Drp1 alone. All GTPase assays have been conducted three times, and the error bars represent SD.

Velocity analytical ultracentrifugation (vAUC). Analytical ultracentrifugation was conducted using a Beckman Proteomelab XL-A and an AN-60 rotor. For sedimentation vAUC, Drp1 and its mutants in S200 buffer (65/150 mM KCl, 1 mM MgCl2, 0.5 mM EGTA, 1 mM DTT, 20 mM HEPES, pH 7.4) was centrifuged at either 5000 (for oligomer) or 35,000 (for monomer) rpm with monitoring at 280 nm. Data analyzed by Sedfit to determine sedimentation coefficient, frictional ratio, and apparent mass. Sedimentation coefficient reported is that of the major peak (at least 80% of the total analyzed mass) at OD_{280}.

High-speed pelleting assay. Interactions between DRP1 actin were tested in the S200 buffer; DRP1 and actin were mixed as described and were incubated for 1 h at room temperature in a 100 μl volume. Interactions between DRP1 Mff were tested in the S200 buffer containing either no nucleotide, 1 mM GMPPCP, or 1 mM GTP. DRP1, nucleotide and Mff were mixed and were incubated for 10 min at 4°C in a 100 μl volume. After incubation, samples were centrifuged at 80,000 rpm for 20 min at 4°C in a TLA-100.1 rotor (Beckman). The supernatant was carefully removed. Pellets were washed three times with S200 buffer and then resuspended in 100 μl of SDS–PAGE sample buffer and resolved by SDS–PAGE (LC6025; Invitrogen, Carlsbad, CA). Gels were stained with Coomassie Brilliant Blue R-250 staining (1610400, Bio-Rad, Hercules, CA), and band intensity was analyzed using ImageJ software. All pelleting assays have been repeated at least two times, and one representative experiment is shown.

ACKNOWLEDGMENTS

We thank Arminja Kettenbach for initial examination of the phosphorylation state of bacterially-expressed Drp1, Noor Taher for help with phospho–proteomic analysis, and Lando Ciripi for exposing himself to the outer surface. This work was supported by National Institutes of Health R01 GM069818 and R35 GM112545 to H.N.H., and National Institutes of Health P20 GM113132 to the BioMT COBRE.

REFERENCES

Abe Y, Wanders RJA, Waterham HR, Mandel H, Falik-Zaccai TC, Ishihara N, Fujiki Y (2023). Genetic defects in peroxisome morphogenesis (Pex11β, dynamin-like protein 1, and nucleoside diphosphate kinase 3) affect docosahexaenoic acid-phospholipid metabolism. J Inherit Metab Dis 46, 273–285.

Adachi Y, Itoh K, Yamada T, Cerveny KL, Suzuki TL, Macdonald P, Frohman MA, Ramachandran R, Iijima M, Sesaki H (2016). Coincident Phosphatidic Acid Interaction Restrains Drp1 in Mitochondrial Division. Mol Cell 63, 1034–1043.

Boissan M, Montagnac G, Shen Q, Griparic L, Guitton J, Romao M, Sauvonnet N, Lagache T, Lascu I, Raposo G, *et al.* (2014). Nucleoside diphosphate kinases fuel dynamin superfamily proteins with GTP for membrane remodeling. Science 344, 1510–1515.

Brand CS, Tan VP, Brown JH, Miyamoto S (2018). RhoA regulates Drp1 mediated mitochondrial fission through ROCK to protect cardiomyocytes. Cell Signal 50, 48–57.

Bui HT, Shaw JM (2013). Dynamin assembly strategies and adaptor proteins in mitochondrial fission. Curr Biol 23, 891–899.

Cereghetti GM, Stangherlin A, de Brito OM, Chang CR, Blackstone C, Bernardi P, Scorrano L (2008). Dephosphorylation by calcineurin regulates translocation of Drp1 to mitochondria. Proc Natl Acad Sci USA 105, 15803–15808.

Chakrabarti R, Ji WK, Stan RV, Sanz JJ, Ryan TA, Higgs HN (2018). INF2-mediated actin polymerization at the ER stimulates mitochondrial calcium uptake, inner membrane constriction, and division. J Cell Biol 217, 251–268.

Chang CR, Blackstone C (2007). Cyclic AMP-dependent protein kinase phosphorylation of Drp1 regulates its GTPase activity and mitochondrial morphology. J Biol Chem 282, 21583–21587.

Chang CR, Blackstone C (2010). Dynamic regulation of mitochondrial fission through modification of the dynamin-related protein Drp1. In: Annals of the New York Academy of Sciences, John Wiley & Sons, 34–39.

Chen CW, Wang HL, Huang CW, Huang CY, Lim WK, Tu IC, Koorapati A, Hsieh ST, Kan SW, Tzeng SR, *et al.* (2019). Two separate functions of NME3 critical for cell survival underlie a neurodegenerative disorder. Proc Natl Acad Sci USA 116, 566–574.

Cho B, Cho HM, Jo Y, Kim HD, Song M, Moon C, Kim H, Kim K, Sesaki H, Rhyu IJ, *et al.* (2017). Constriction of the mitochondrial inner compartment is a priming event for mitochondrial division. Nat Commun 8, 15754.

Clinton RW, Francy CA, Ramachandran R, Qi X, Mears JA (2016). Dynamin-related protein 1 oligomerization in solution impairs functional interactions with membrane-anchored mitochondrial fission factor. J Biol Chem 291, 478–492.

Connor OM, Matta SK, Friedman JR (2023). Completion of mitochondrial division requires the intermembrane space protein Mdi1/Atg44. J Cell Biol 222, e202303147.

Cribbs JT, Strack S (2007). Reversible phosphorylation of Drp1 by cyclic AMP-dependent protein kinase and calcineurin regulates mitochondrial fission and cell death. EMBO Rep 8, 939–944.

Fröhlich C, Grabiger S, Schwefel D, Faelber K, Rosenbaum E, Mears J, Rocks O, Daumke O (2013). Structural insights into oligomerization and mitochondrial remodelling of dynamin 1-like protein. EMBO J 32, 1280–1292.

Galvan DL, Long J, Green N, Chang BH, Lin JS, Schumacker P, Truong LD, Overbeek P, Danesh FR (2019). Drp1S600 phosphorylation regulates mitochondrial fission and progression of nephropathy in diabetic mice. J Clin Invest 129, 2807–2823.

Han H, Tan J, Wang R, Wan H, He Y, Yan X, Guo J, Gao Q, Li J, Shang S, *et al.* (2020). PINK1 phosphorylates Drp1^{S616} to regulate mitophagy-independent mitochondrial dynamics. EMBO Rep 21, e48686.

Han XJ, Lu YF, Li SA, Kaitsuka T, Sato Y, Tomizawa K, Nairn AC, Takei K, Matsui H, Matsushita M (2008). CaM kinase Iα-induced phosphorylation of Drp1 regulates mitochondrial morphology. J Cell Biol 182, 573–585.

Harris ES, Higgs HN (2006). Biochemical analysis of mammalian formin effects on actin dynamics. Methods Enzymol 406, 190–214.

Hatch AL, Ji WK, Merrill RA, Strack S, Higgs HN (2016). Actin filaments as dynamic reservoirs for Drp1 recruitment. Mol Biol Cell 27, 3109–3121.

Honsho M, Abe Y, Imoto Y, Chang ZF, Mandel H, Falik-Zaccai TC, Fujiki Y (2020). Mammalian homologue nme3 of dynamo1 regulates peroxisome division. Int J Mol Sci 21, 1–21.

Ikeda A, Iijima M, Sesaki H (2023). A nucleotide diphosphate kinase mediates tethering between mitochondria prior to fusion. J Cell Biol 222, e202309037.

Itoh K, Adachi Y, Yamada T, Suzuki TL, Otomo T, McBride HM, Yoshimori T, Iijima M, Sesaki H (2018). A brain-enriched drp1 isoform associates with lysosomes, late endosomes, and the plasma membrane. J Biol Chem 293, 11809–11822.

Jhun BS, O-Uchi J, Adaniya SM, Mancini TJ, Cao JL, King ME, Landi AK, Ma H, Shin M, Yang D, *et al.* (2018). Protein kinase D activation induces mitochondrial fragmentation and dysfunction in cardiomyocytes. J Physiol 596, 827–855.

Ji WK, Hatch AL, Merrill RA, Strack S, Higgs HN (2015). Actin filaments target the oligomeric maturation of the dynamin GTPase Drp1 to mitochondrial fission sites. Elife 4, e11553.

Ji WK, Chakrabarti R, Fan X, Schoenfeld L, Strack S, Higgs HN (2017). Receptor-mediated Drp1 oligomerization on endoplasmic reticulum. J Cell Biol 216, 4123–4139.

Kalia R, Wang RYR, Yusuf A, Thomas PV, Agard DA, Shaw JM, Frost A (2018). Structural basis of mitochondrial receptor binding and constriction by DRP1. Nature 558, 401–405.

Kashatus JA, Nascimento A, Myers LJ, Sher A, Byrne FL, Hoehn KL, Counter CM, Kashatus DF (2015). Erk2 phosphorylation of Drp1 promotes mitochondrial fission and MAPK-driven tumor growth. Mol Cell 57, 537–551.

Koirala S, Guo Q, Kalia R, Bui HT, Eckert DM, Frost A, Shaw JM (2013). Interchangeable adaptors regulate mitochondrial dynamin assembly for membrane scission. Proc Natl Acad Sci 110, 1342–1351.
Korobova F, Ramabhadran V, Higgs HN (2013). An actin-dependent step in mitochondrial fission mediated by the ER-associated formin INF2. Science (80-) 339, 464–467.
Kraus F, Roy K, Pucadyil TJ, Ryan MT (2021). Function and regulation of the divisome for mitochondrial fission. Nature 590, 57–66.
Liu A, Kage F, Higgs HN (2021). Mff oligomerization is required for Drp1 activation and synergy with actin filaments during mitochondrial division. Mol Biol Cell 32, ar5.
Liu A, Kage F, Sapp G, Aydin H, Higgs HN (2023). Long-chain fatty acyl-coenzyme A activates the mitochondrial fission factors MiD49 and MiD51 by inducing their oligomerization. BioRxiv, 2023.07.31.551267.
Liu R, Chan DC (2015). The mitochondrial fssion receptor Mff selectively recruits oligomerized Drp1. Mol Biol Cell 26, 4466–4477.
Losón OC, Song Z, Chen H, Chan DC (2013). Fis1, Mff, MiD49, and MiD51 mediate Drp1 recruitment in mitochondrial fission. Mol Biol Cell 24, 659–667.
Macdonald PJ, Stepanyants N, Mehrotra N, Mears JA, Qi X, Sesaki H, Ramachandran R (2014). A dimeric equilibrium intermediate nucleates Drp1 reassembly on mitochondrial membranes for fission. Mol Biol Cell 25, 1905–1915.
Montecinos-Franjola F, Bauer BL, Mears JA, Ramachandran R (2020). GFP fluorescence tagging alters dynamin-related protein 1 oligomerization dynamics and creates disassembly-refractory puncta to mediate mitochondrial fission. Sci Reports 10, 1–16.
Osellame LD, Singh AP, Stroud DA, Palmer CS, Stojanovski D, Ramachandran R, Ryan MT (2016). Cooperative and independent roles of the Drp1 adaptors Mff, MiD49 and MiD51 in mitochondrial fission. J Cell Sci 129, 2170–2181.
Perez-Riverol Y, Bai J, Bandla C, García-Seisdedos D, Hewapathirana S, Kamatchinathan S, Kundu D, Prakash A, Frericks-Zipper A, Eisenacher M, *et al*. (2022). The PRIDE database resources in 2022: A hub for mass spectrometry-based proteomics evidences. Nucleic Acids Res 50, D543–D552.
Qi X, Disatnik M-H, Shen N, Sobel RA, Mochly-Rosen D (2011). Aberrant mitochondrial fission in neurons induced by protein kinase Cδ under oxidative stress conditions in vivo. Mol Biol Cell 22, 256–265.
Rosdah AA, Smiles WJ, Oakhill JS, Scott JW, Langendorf CG, Delbridge LMD, Holien JK, Lim SY (2020). New perspectives on the role of Drp1 isoforms in regulating mitochondrial pathophysiology. Pharmacol Ther. 213, 107594.
Serasinghe MN, Wieder SY, Renault TT, Elkholi R, Asciolla JJ, Yao JL, Jabado O, Hoehn K, Kageyama Y, Sesaki H, Chipuk JE (2015). Mitochondrial division is requisite to RAS-induced transformation and targeted by oncogenic MAPK pathway inhibitors. Mol Cell 57, 521–536.
Spudich JA, Watt S (1971). The regulation of rabbit skeletal muscle contraction. I. Biochemical studies of the interaction of the tropomyosin-troponin complex with actin and the proteolytic fragments of myosin. J Biol Chem 246, 4866–4871.
Strack S, Wilson TJ, Cribbs JT (2013). Cyclin-dependent kinases regulate splice-specific targeting of dynamin-related protein 1 to microtubules. J Cell Biol 201, 1037–1051.
Taguchi N, Ishihara N, Jofuku A, Oka T, Mihara K (2007). Mitotic phosphorylation of dynamin-related GTPase Drp1 participates in mitochondrial fission. J Biol Chem 282, 11521–11529.
Valera-Alberni M, Joffraud M, Miro-Blanch J, Capellades J, Junza A, Dayon L, Galiindo AN, Sanchez-Garcia JL, Valsesia A, Cercillieux A, *et al*. (2021). Crosstalk between Drp1 phosphorylation sites during mitochondrial remodeling and their impact on metabolic adaptation. Cell Rep 36, 109565.
Wang W, Wang Y, Long J, Wang J, Haudek SB, Overbeek P, Chang BHJ, Schumacker PT, Danesh FR (2012). Mitochondrial fission triggered by hyperglycemia is mediated by ROCK1 activation in podocytes and endothelial cells. Cell Metab 15, 186–200.
Warnock DE, Hinshaw JE, Schmid SL (1996). Dynamin self-assembly stimulates its GTPase activity. J Biol Chem 271, 22310–22314.
Wikstrom JD, Israeli T, Bachar-Wikstrom E, Swisa A, Ariav Y, Waiss M, Kaganovich D, Dor Y, Cerasi E, Leibowitz G (2013). AMPK regulates ER morphology and function in stressed pancreatic β-cells via phosphorylation of DRP1. Mol Endocrinol 27, 1706–1723.
Wilson TJ, Slupe AM, Strack S (2013). Cell signaling and mitochondrial dynamics: Implications for neuronal function and neurodegenerative disease. Neurobiol Dis 51, 13–26.
Xu S, Wang P, Zhang H, Gong G, Gutierrez Cortes N, Zhu W, Yoon Y, Tian R, Wang W (2016). CaMKII induces permeability transition through Drp1 phosphorylation during chronic β-AR stimulation. Nat Comm, 7, 1–13.
Yu R, Liu T, Ning C, Tan F, Jin SB, Lendahl U, Zhao J, Nistér M (2019). The phosphorylation status of Ser-637 in dynamin-related protein 1 (Drp1) does not determine Drp1 recruitment to mitochondria. J Biol Chem 294, 17262–17277.
Yu T, Jhun BS, Yoon Y (2011). High-glucose stimulation increases reactive oxygen species production through the calcium and mitogen-activated protein kinase-mediated activation of mitochondrial fission. Antioxidants Redox Signal 14, 425–437.